Radiatively Active Hydrometeors Frequencies from CloudSat-CALIPSO Data for Evaluating Cloud Fraction in Global Climate Models

Li, Jui-Lin F.[1,2], **Wei-Liang Lee[3], Kuan-Man Xu[4], Yu-Cian Tsai[5], Jonathon Jiang[1], Jia-Yuh Yu[5], Graeme Stephens[1], Eric Fetzer[1,2], W-T Chen[6]

[1]Jet Propulsion Laboratory, California Institute of Technology, Pasadena, CA, USA
[2]Joint Institute for Regional Earth System Science and Engineering, University of California, Los Angeles, CA, USA
[3]Research Center for Environmental Changes, Academia Sinica, Taipei, Taiwan
[4]Science Directorate, NASA Langley Research Center, Hampton, VA, USA
[5]Department of Atmospheric Sciences, National Central University, Taoyuan City, Taiwan
[6]Department of Atmospheric Sciences, National Taiwan University, Taipei City, Taiwan

Submitted to *J. Geophys. Res. Atmos.*

Jet Propulsion Laboratory/NASA, CalTech

2022

**Corresponding Author: Wei-Liang Lee: leelupin@gate.sinica.edu.tw

Abstract

This study derives radiatively-active hydrometeors frequencies (HFs) from CloudSat-CALIPSO satellite data to evaluate cloud fraction in present-day simulations by CMIP5 models. Most CMIP5 models do not consider precipitating and/or convective hydrometeors but CESM1-CAM5 in CMIP5 has diagnostic snow and CESM2-CAM6 in CMIP6 has prognostic precipitating ice (snow) included. However, the models do not have snow fraction available for evaluation. Since the satellite-retrieved hydrometeors include the mixtures of floating, precipitating and convective ice and liquid particles, a filtering method is applied to produce estimates of cloud-only HF (or NPCHF) from the total radiatively-active HF (THF), which is the sum of NPCHF, precipitating ice HF and convective HF. The reference HF data for model evaluation include estimates of liquid-phase NPCHF from CloudSat radar-only data (2B-CWC) and ice-phase THF from CloudSat-CALIPSO 2C-ICE combined radar/lidar data. The model evaluation results show that cloud fraction from CMIP5 multi-model mean (MMM) is significantly underestimated (up to 30 %) against the total HF estimates, mainly below the mid-troposphere over the extratropics and in the upper-troposphere over the midlatitude lands and a few tropical convective regions. The CMIP5 cloud fraction biases are reduced dramatically when compared to the cloud-only HF estimates, but the area of overestimates expands from the tropical convective regions to mid-latitudes in the lower and upper troposphere. There is no CMIP5 standard output snow fraction available for comparison against CloudSat-CALIPSO estimate. The implications of these results show that hydrometeors frequency estimates from CloudSat-CALIPSO provide a reference for GCM's cloud fraction from stratiform and convective form.

The three key points:

Key point #1: Deriving non-precipitating and non-convective (cloud only) and total radiatively-active hydrometeor frequency (HF) from CloudSat-CALIPSO data.

Key point #2: Cloud fractions from CMIP5 multi-model-mean compare well to cloud-only HF estimates, implying severely underestimated against total HF estimates.

Key point #3: Hydrometeors frequency estimates from CloudSat-CALIPSO provides a reference for GCM's cloud fraction from stratiform and convective form.

1. Introduction

Both the frequency and mass of radiatively active hydrometeors, including floating cloud ice and liquid, precipitating hydrometeors (snow), and convective ice and liquid, are important for atmospheric shortwave (SW) and longwave (LW) radiation computation (Li et al., 2013, 2018; Waliser et al., 2011; Gettelman et al., 2010; Gettelman and Morrison, 2015; Michibata et al., 2019). However, most general circulation models (GCMs), such as those participating in the 5th phase of Coupled Model Intercomparison Project (CMIP5) (Taylor et al., 2001; Gleckler et al., 2011), and the 6th phase (CMIP6) (except the CESM2-CAM6 family that considers snow-radiative effects) only consider the mass and frequency of floating cloud ice and liquid, ignoring radiatively important precipitating hydrometeor and convective core hydrometeor. Thus, the modeled atmospheric heating profiles and possibly the global radiation balance may be impacted by the missing hydrometeors because atmospheric radiation is sensitive to the broader range of hydrometeors (Li et al., 2012; Waliser et al., 2009). The miscounted or misrepresented mass of precipitating ice and convective core hydrometeors result in underestimated total ice water content and path (Li et al., 2012), which are expected to contribute to model biases of radiation budget (Li et al., 2013). Our previous studies have been focusing on characterizing and diagnosing systematic biases in the CMIP3/CMIP5/CMIP6 models associated with the precipitating ice radiative effects as well as the biases in weather models such as the European Centre for Medium-range Weather Forecast (ECMWF) (Li et al., 2014b). For example, these biases produce underestimated land surface temperature (Li et al., 2016b), overestimated sea ice concentration (Li et al., 2022) and have impacts on the modeled sea surface temperatures (Li et al., 2014a, 2016a, b, 2021).

While the aforementioned systematic biases contributed by ignoring the precipitating hydrometeors mass exist in many GCMs, it is essential to evaluate their performance in terms of

the frequency (fraction) of radiatively active hydrometeors because it also contributes to atmospheric radiation in GCMs. However, satellite observations (e.g., CloudSat and CALIPSO) only provide retrievals of the total water mass for liquid and ice, which is the sum of floating water/ice and precipitating water/ice in stratiform clouds and convective cores (Li et al., 2012). Therefore, they are not suitable for direct comparisons with the mass and frequency of non-precipitating and non-convective hydrometeors produced by most GCMs. To separate the floating cloud ice from precipitation and convective cores, Chen et al. (2011) and Li et al. (2012) developed filtering methods to provide (floating) cloud ice water content (CIWC). These concepts and datasets have been widely employed by the scientific community. For example, Gettelman et al. (2010) used CIWC to evaluate new ice cloud microphysical approaches for the Community Atmosphere Model version 5 in the Community Earth System Model version 1 (CESM1-CAM5) and to develop a new convection scheme with convective cloud ice mass included in CAM5 (Song et al., 2012). Zhang et al. (2014) investigated ice nucleation in cirrus clouds. The dataset has also been used to evaluate the IWC representation in the UCLA GCM (Ma et al., 2012), the Weather Research and Forecasting (WRF) model (Wu et al., 2015), and the Goddard Multiscale Modeling System (Tao et al., 2009). Another approach is to use satellite simulator software for model assessment (Bodas-Salcedo et al., 2011), such as using the GCM-Oriented CALIPSO Cloud Product (CALIPSO-GOCCP) (Cesana et al., 2016), and to evaluate model's cloud phase transition and low cloud feedback (Cesana et al., 2019). But this approach does not separate the different types of hydrometeors frequency and might miss the frequency of large particles, which are detected by CloudSat radar but not by CALIPSO lidar (Cesana et al., 2019).

It is noted that the aforementioned studies have focused on the mass and radiative effects of cloud and precipitating hydrometeors. In this study, we turn our perspective to the occurrence

of the radiatively active hydrometeor frequency (HF), which is generally considered equivalent to the cloud fraction except for sampling cloud fields at a fixed location in time (Clothiaux et al., 2009; Xu et al., 2012) or on a narrow satellite swath in space such as CloudSat and CALIPSO. The objective of this study is to provide an observational estimate to evaluate different types of HF (cloud fraction in model output), including cloud ice, precipitating ice, and cloud liquid, from the CMIP5 models. Three retrieval algorithms, either using CloudSat radar or CALIPSO lidar or both, provide global retrievals of ice water content (IWC), including small particles (floating cloud ice) to larger particles (snow), and liquid water content (LWC), as well as the effective radius (Re) and the extinction coefficient from the thinnest cirrus (seen only by the lidar) to the thickest ice cloud (Austin et al., 2001; Hogan et al., 2006; Delanoë and Hogan, 2008, 2010; Macc et al., 2009; Young and Vaughan, 2009; Sassen et al., 2009; Deng et al., 2010; Stein et al., 2011). In this study, we use cloud liquid HF from CloudSat-only 2B-CWC-RO5 product (Austin et al., 2009; Li et al., 2018), combined with CloudSat-CALIPSO ice water products from 2C-ICE (Deng et al., 2010, 2013) and DARDAR (raDAR/liDAR) (Hogan, 2006; Delanoë and Hogan, 2008, 2010) for obtaining the total HF (THF), non-precipitating and non-convective HF (NPCHF), precipitating ice HF (PIHF), and convective HF (CHF), so that a robust and meaningful observational HF estimate can be made for model evaluations.

In Section 2, we describe the observational resources for the estimated hydrometeor frequency from CloudSat-CALIPSO data, the separation of different types of hydrometeor frequencies and the cloud fractions in model simulations. In Section 3, we discuss the results with a summary and conclusions drawn in Section 4.

2. Reference Datasets, Separation of Hydrometeors Frequency and Model output

2.1 Hydrometeors Frequency Reference Datasets

We generate five types of HF, based on the "FLAG" method developed in Waliser et al. (2009) and Li et al. (2012, 2018), for non-precipitating and non-convective floating cloud ice (FIHF) and cloud liquid (FLHF), convective ice (CIHF) and convective liquid (CLHF), and precipitating ice (PIHF) associated with their respective masses, using CloudSat-CALIPSO measurements including 2B-CWC, 2C-ICE, and DARDAR datasets. The sum of FIHF and FLHF is also called, interchangeably, non-precipitating and non-convective HF (NPCHF) or cloud-only HF. These three datasets cover the period of January 2007 to December 2010.

(a) *2B-CWC-RO5* (Austin et al., 2001, 2009) is a CloudSat-only product that provides estimates of the hydrometeor content from measured radar reflectivity to constrain the retrieved mass of both liquid and ice phases for all heights.

(b) *DARDAR* (raDAR/liDAR) (Hogan, 2006; Delanoë and Hogan, 2008, 2010) is a synergistic ice cloud retrieval product derived from the combination of the CloudSat radar and CALIPSO lidar using a variational method for retrieving profiles of the extinction coefficient, IWC, and equivalent radius (Re) of the ice cloud (Brown and Francis, 1995; Francis et al., 1998; Delanoë et al., 2011; Stein et al., 2011; Delanoë and Hogan, 2010).

(c) *2C-ICE* (Deng et al., 2010) provides ice cloud retrieval also derived from the combination of the CloudSat radar and CALIPSO lidar. While using the same satellite input, 2C-ICE is different from DARDAR in many ways, such as the vertical resolution, treatments of multiple scattering and backscattering, and assumptions of the particle size distribution. Readers desiring a more in-depth description of the 2C-ICE algorithm should refer to Deng et al. (2010, 2013) for details.

2.2 Separation of Hydrometeors Frequency

There are two essential aspects regarding the compatibility of the hydrometeor mass and frequency between model and observation. First, CALIPSO measurements used in the DARDAR and 2C-ICE products have more sensitivity to small and thin cirrus clouds that might make very little contribution to the total ice mass and water content of clouds but could play an important role in the radiation budget (Liou, 1986, 2002; Sassen, 2003; Schumann, 2002, 2009). Second, more importantly, all three products, to first order, represent the total tropospheric ice/liquid, including "floating" cloud ice/liquid and the precipitating ice (snow) with variable sizes and terminal velocities as the combined measurements are sensitive to a wide range of particle sizes. The particle sizes, including those of particles associated with convective clouds, are generally not included as prognostic variables in all current GCMs (e.g., Li et al., 2012; Waliser et al., 2009). Furthermore, it is generally assumed that convective core areas are small relative to a grid box in a typical GCM grid box size larger than a few hundred km^2. Thus, its contribution to HF and mass is not very large. Even if it is either prognostically or diagnostically determined, the relative contribution does not change. However, as the resolution in the most current state-of-the-art GCMs become higher, with grid box size smaller than 100 km^2 to tens of km^2, the contribution of HF and mass of the convective cores should be considered.

In this study, we use the "FLAG-method," following Waliser et al. (2009) and Li et al. (2012), to distinguish HFs associated with clouds with ice/liquid mass from HFs associated with precipitation and convection. This method is summarized as follows. To achieve the separation of HFs of different types, we exclude all the retrievals in any profile that are flagged as precipitating at the surface and any retrieval within the profile whose cloud type is classified as "deep convection" or "cumulus" (from CloudSat 2B-CLDCLASS dataset; Sassen and Wang, 2008). The remaining profiles are associated with clouds with floating ice/liquid mass. Their frequencies are

called either floating ice HF (FIHF) or floating liquid HF (FLHF), depending on the cloud phase. The frequencies of the excluded profiles associated with precipitation are called precipitating ice HF (PIHF) while precipitating liquid (rain) is not important for radiative calculation, which will not be discussed. The frequencies of the excluded profiles associated with convection are called either convective ice HF (CIHF) or convective liquid HF (CLHF), depending upon the cloud phase. The total ice hydrometeor frequency (TIHF) is the sum of FIHF, PIHF and CIHF while the total liquid HF (TLHF) is the sum of FLHF and CLHF. This methodology was used for estimating CIWP/CIWC used for CMIP3 model-data comparisons (e.g., Li et al., 2012; Waliser et al., 2009) and for model cloud parameterizations improvements in CAM5 (Gettelman et al., 2010; Song et al., 2011), as well as other applications mentioned in the introduction.

The caveat of the aforementioned HF separation method that we need to keep in mind is that it is impossible to completely separate floating/cloudy forms from precipitating forms, as they coexist at some height intervals. Specific retrievals of this sort will require co-located vertical velocity information, such as from a Doppler radar capability and/or a multiple frequency radar, to better characterize particle sizes that are not available yet. Thus, it is beyond the scope of this study.

2.3 Cloud Fraction in GCMs

The protocol output of cloud fraction from all CMIP5 models only includes “cloud only” fraction, which is equivalent to non-precipitating and non-convective HF (NPCHF) from observational estimate outlined above. Some CMIP5 models do consider convective ice and/or diagnostic precipitating ice (snow) hydrometeors such as CESM1-CAM5, however, the model does not have snow fraction output available. The CMIP5 simulations used in this study are listed in Table A1, which provides an outline of cloud microphysics parameterizations used in each

model. The historical simulation, which used observed 20th-century greenhouse gases, ozone, aerosol, and solar forcing, is analyzed. The period used for the long-term mean is 1970-2005, and if a model provided multiple members of simulations, only one of them was chosen for this evaluation. For the purposes of comparison, both the GCM and observational datasets are re-gridded into a common horizontal grid of 2° latitude by 2° longitude. Figure 1h shows the zonally-averaged cloud fraction (ice+liquid) distribution from the CMIP5 multi-model-mean (MMM).

In addition to the CMIP5 model output, we also discuss the CESM2-CAM6 model output. The CAM6 implements a new prognostic cloud microphysics scheme for cloud ice, liquid, precipitating ice, and rain (Gettelman and Morrison, 2015; MG2). However, the model does not provide comparable output for snow fraction for comparisons.

3. Results

3.1 Observational Estimates of Hydrometeor Frequencies

To account for the observational uncertainty of HFs, we produce three different estimates of HFs from 2B-CWC, 2C-ICE, and DARDAR datasets in this study. Shown in Figure 2 are the zonally-averaged HFs determined by nonzero radar/lidar reflectivity from CloudSat/CALIPSO data with the classification of precipitation and convection based on surface precipitation and convective cloud flags, respectively. These are averaged from 2007 to 2010 in time. These HFs include total ice HF (TIHF; panels a, f and k), which is the sum of precipitating ice HF (PIHF; panels b, g and l), convective ice HF (CIHF; panels c, h and m), and floating cloud ice frequency (FIHF; panels e, j and o). Panels d, i and n show the sum of PIHF and CIHF. Figures 2a-2g are for 2B-CWC, Figures 2f—2j are for 2C-ICE, and Figures 2k—2o are for DARDAR.

Overall, the precipitating ice HF dominates the total ice HF; i.e., PIHF is 22—26% below 400 hPa, compared to 30—40% of TIHF over the mid-latitudes of both hemispheres (Figures 2b,

2g, 2l). The convective ice HF (CIHF) contributes about 6—8% between 350—500 hPa from the tropical convective zones (Figures 2c, 2h, 2m). Cloud-only ice HF (FIHF) (Figures 2e, 2j, 2o) represents 10—26% contribution, which is smaller than the PIHF over the mid-latitudes. But FIHF is larger in the upper troposphere over the tropics and midlatitudes. This is especially true for 2C-ICE and DARDAR datasets because thin ice clouds can be detected by CALIPSO lidar, but not by CloudSat radar (2B-CWC). Nevertheless, the differences in PIHF between 2C-ICE and DARDAR, as discussed below, are much smaller, compared to their differences with 2B-CWC.

To see the differences between the three datasets, the total ice HF and floating ice HF differences are calculated between 2C-ICE and 2B-CWF (Figures 3a and 3b), between DARDAR and 2B-CWC (Figures 3c and 3d) and between 2C-ICE and DARDAR (Figures 3e and 3f). It is evident that TIHF (Figure 3a and 3c) and FIHF (Figure 3b and 3d) estimates from the 2C-ICE and DARDAR datasets are much larger above 300-hPa levels over the tropics and above 500-hPa levels over the mid-latitudes than the radar-only 2B-CWC data. This is due to the fact that most small ice particles in cirrus clouds detected by CALIPSO lidar (2C-ICE and DARDAR) are invisible to CloudSat radar (2B-CWC), resulting in minimal amounts of HF in 2B-CWC over the upper troposphere. Since the TIHF and FIHF differences between 2C-ICE and DARDAR datasets (Figure 3e and 3f) are only ~2%, we will use 2C-ICE as our reference to compare the observed frozen hydrometeors frequencies (i.e., FIHF, PIHF and TIHF) with CMIP5 models in this study. As discussed later, the differences in HFs between models and observational estimates are much larger than 2%.

We also generate estimates of total liquid HF (TLHF), precipitating liquid HF (PLHF), and floating cloud liquid HF (FLHF) based on 2B-CWC dataset, which are shown in Figures 4a-c. They, as expected, have large values in the lower troposphere but not detected below ~900 hPa

238 due to ground clutter effects of CloudSat radar. The maximum FLHF occurs between 800—900
239 hPa in the midlatitudes while the smallest FLHP occurs above ~800 hPa in the subtropics of both
240 hemispheres due to large-scale subsidence. Note that the precipitating liquid (rain) is not
241 radiatively active due to its large particle size. Therefore, only FLHF and convective liquid HF are
242 considered as parts of the total HF in this study.

243 To get the total HF (THF), we add float liquid HF (FLHF) to total ice HF (TIHF). We also
244 add FLHF to float ice HF (FIHF) to produce the estimate of non-precipitating and non-convective
245 HF (NPCHF), total floating HF (TFHF) or cloud-only HF. The zonally-averaged annual mean
246 THF and NPCHF are shown for 2B-CWC (Figure 1a, b), for 2C-ICE (Figure 1c, d), and DARDAR
247 (Figure 1e, f), respectively. These estimated HFs can be used as references for evaluating cloud
248 fractions in GCMs. The comparisons with GCMs are shown in the following sections.

249 ***3.2 Comparison of zonally-averaged hydrometeor frequency***

250 Figure 5 shows the differences of CMIP5-MMM cloud fractions from the combined THF
251 and NPCHF estimates of frozen HFs from Cloudsat-CALIPSO 2C-ICE and floating liquid HF
252 from 2B-CWC, which are used as the reference data. Differences for CMIP5-MMM from other
253 reference data are shown in Figure A1. The zonally-averaged CMIP5-MMM cloud fraction is
254 substantially smaller than the estimated THF by up to 20—60% over the southern and northern
255 hemisphere mid- and high-latitudes, as shown in Figure 5a. On the contrary, it is reasonably well
256 described compared to the estimated NPCHF with biases within 5% (Figure 5b). The excessive
257 cloud fraction in the mid-troposphere of the tropics might be due to the uncertainty of the
258 missing/undetected hydrometeors from CloudSat-CALIPSO caused by the strong attenuation of
259 radar/lidar signals under thick convective cloud regions.
260

3.3 Comparison of regionally averaged profiles of hydrometeor frequency

Figure 6 shows the profiles of regional area averages of CMIP5-MMM cloud fractions against the estimated NPCHF and THFs for the globe [panels (a) and (b): 80°S—80°N], tropics [panels (c) and (d): 30°S—30°N], northern hemisphere (NH) mid-latitudes [panels (e) and (f): 30°N—60°N] and high-latitudes belts [panels (i) and (j): 60°N—80°N], and southern hemisphere (SH) mid-latitudes [panels (g) and (h): 30°S—60°S] and high-latitudes belts [panel (k) and (l): 60°S—80°S).

In general, the mean cloud fractions from CMIP5-MMM over all the above-mentioned regions agree well to the estimated cloud-only HF (NPCHF) with biases within 5%, as shown in the lower panels of Figure 6. When compared to the estimated THF, the mean CMIP5-MMM cloud fractions are underestimated below 300 hPa for all the above-mentioned regions because CMIP5 models do not have precipitating ice and convective cloud hydrometeors included in cloud fractions. That is, precipitating ice and convective cores do not impact radiative calculation in these models. The maximum magnitudes of underestimated CMIP5 cloud fractions could reach up to 20—25% for mid- and high-latitudes over both hemispheres (Figures 6g, 6h, 6i, 6j, 6k, 6l), mainly due to the lack of precipitating ice cloud fractions. In reality, they are contributed by mid- and high-latitudes storms and stratiform precipitating ice over the polar regions.

3.4. Comparison of horizontal distributions of hydrometeor frequency

Figure 7 shows the CMIP5-MMM cloud fraction biases at 700 hPa, 500 hPa, and 300 hPa against the estimated THF (Figures 7a, 7d and 7g) and NPCHF (Figures 7b, 7e and 7h). As shown in Figure 7a, at 700 hPa, it is evident that CMIP5-MMM substantially underestimates the THF

north of 40°N and south of 40°S over storm tracks and the Arctic and Antarctic regions due to the lack of precipitating ice in CMIP5 models. The slightly overestimated CMIP5-MMM cloud fractions over convective zones might be due to the strong attenuation of radar signals below thick convective clouds that are not detected by the CloudSat radar. Compared to the estimated cloud-only HF, CMIP5-MMM cloud fractions are overestimated over the convective zones and storm track regions but still underestimated in the polar regions, as shown in Figure 7b. In general, CMIP5-MMM cloud fractions at 700 hPa are very close to the estimated NPCHF with magnitude differences less than 8%.

At 500 hPa, the CMIP5-MMM cloud fractions are generally underestimated over mid- and high-latitudes storm tracks and over convectively active regions such as the ITCZ, SPCZ, and warm pool due to the lack of stratiform precipitating ice and convective ice, compared to the estimated THF, as shown in Figure 7d. In contrast, they show very small biases against the estimated NPCHF with biases less than 2.5% (Figure 7e).

At 300 hPa, the CMIP5-MMM cloud fractions are slightly underestimated (-2.5 — -8%) against the estimated THF (Figure 7g). The largest underestimates occur in places where precipitating ice HF is expected to be large; for example, over the storm track in the North Pacific, midlatitude lands and convectively-active regions over the SPCZ and warm pool. Interestingly, the CMIP5-MMM cloud fractions are larger than the estimated THF over the South Pacific trade-wind regions and the Southern Ocean, indicating that the CMIP5 models simulate excessive high clouds over these regions (Figure 7g and 7h). This feature over the trade-wind regions is not shown over the zonally-averaged profiles (Figures 5a, 5b and 6) due to the cancellation associated with underestimates over the SPCZ. In our previous study (Li et al., 2021), we attributed this excessive cloud fraction in CMIP5-MMM to hydrometeor-radiation-circulation coupling biases caused by

the lack of precipitating ice radiative effects over the convective regions, leading to weaker surface wind stress, weaker trade-winds speed (effectively moist and warm advection into the region) and warmer SSTs, consequently producing high-level convective clouds over the trade-wind regions. It seems that the southeast Pacific trade-wind region does not have clouds at 300 hPa or not as much as those in CMIP5-MMM.

4. Summary and Conclusions

The radiative properties of hydrometeors that are input to radiative calculation in GCMs include the mass and hydrometeors occurrence frequency. The purpose of this study is to make judicious comparisons and evaluations of the GCM representations of cloud fraction against the satellite observations of radiatively-active hydrometeor frequencies, which are inherently the combination of cloud-only ice/liquid and precipitating ice (snow). We employ a set of satellite observations of hydrometeors, including 2B-CWC-RO5 from the CloudSat radar for cloud liquid frequency and 2C-ICE and DARDAR from the combined CloudSat radar and CALIPSO lidar retrievals for frequency of cloud ice and precipitating ice (snow+graupel+hail). Then the FLAG method developed by Li et al. (2012) is used to categorize different types of hydrometeors frequency for floating cloud liquid/ice, precipitating ice, and convective liquid/ice.

We examined the annual-mean zonally averaged hydrometeor frequency estimates from the 2B-CWC, 2C-ICE, and DARDAR datasets. The HF derived from the 2B-CWC radar only data does not detect small ice particles such as suspended thin cirrus while it can be captured by the CALIPSO lidar used in the 2C-ICE and DARDAR datasets. It is noted that the differences in frozen hydrometeors and total hydrometeor frequencies are trivial between 2C-ICE and DARDAR. Therefore, we choose ice HF of 2C-ICE and liquid HF from 2B-CWC as a reference

for evaluating model simulation of cloud fraction. The filtered frequency of non-precipitating and non-convective hydrometeors (NPCHF, also called cloud-only HF) and total HF (THF), which is the sum of NPCHF, convective liquid/ice and precipitating ice (snow) HFs, can be utilized for a sensible "apple to apple" comparison within the limitation of measurement accuracy for models that produce either cloud-only cloud fraction (CMIP5 models) or cloud fraction with snow considered for computing the associated radiative effects in GCMs (such as in CESM2-CAM6 in CMIP6), respectively. Note that the precipitating liquid (rain) is not radiatively active in all current GCMs except in new version of GISS-E3 (Li et al., 2022). However, there is no snow fraction output available in CESM2-CAM6 for model-data comparison. In this study, we can only do the model-data evaluation for cloud-only liquid and ice frequency (fraction) in the CMIP5 models.

We evaluated zonally-averaged cloud (only) fraction from multi-model-mean (MMM) of CMIP5 historical simulations during 1970—2005 against the estimated THF and cloud-only HF. The performance of simulated CMIP5-MMM cloud fraction is extremely well in comparison to the estimated cloud-only HF with biases within 5%, except for some overestimates over the midlatitudes of both hemispheres, probably due to the attenuation of radar/lidar signals by thick clouds. When compared to the total HF (THF), CMIP5-MMM cloud fraction is underestimated with biases more than 30% magnitudes over the mid- to high-latitudes and the deep tropics below 700 hPa due to the lack of precipitating ice in the CMIP5 models. The underestimates are drastically reduced over the high latitudes, compared to CMIP5-MMM.

We further examined the hydrometeor frequency of the CMIP5 in terms of regionally area-averaged profiles of CMIP5-MMM cloud fraction against the estimated cloud-only and total HF for global, tropical, and mid- and high-latitudes belts. We found that the performance of CMIP5-MMM is very good for all regions against the estimated cloud-only HF profiles, agreeing with

each other with biases within 5%. However, compared to the estimated total HF (THF) profiles, all regionally-averaged profiles of CMIP5-MMM HF are significantly underestimated (20—25%) because the CMIP5 models do not have precipitating ice and convective hydrometeors, in particular, over the mid- and high-latitude belts and stratiform precipitating ice over the polar latitudes.

To better understand the characteristics of cloud fraction biases, we examined the spatial patterns of CMIP5-MMM cloud fraction biases against the estimated cloud-only and total HFs at 700 hPa, 500 hPa, and 300 hPa. Compared to the total HF, the CMIP5-MMM cloud fraction at 700 hPa is underestimated by as large as 25% north of 40°N and south of 40°S, including storm tracks and the Arctic and Antarctic regions, due to the lack of precipitating ice in CMIP5-MMM. It is also underestimated everywhere at 500 hPa with smaller biases than at 700 hPa and slightly underestimated over the northern hemisphere midlatitudes and SPCZ. On the other hand, CMIP5-MMM cloud fraction is overestimated over the tropical convective zones, probably caused by attenuation of radar signals below thick convective clouds. Compared to the estimated cloud-only HF at 700 hPa, the CMIP5-MMM cloud fraction biases are reduced significantly over the polar regions and it is also reduced everywhere at 500 hPa with biases less than 2.5%, but areas with overestimates increase from the tropical convective regions to the middle latitudes at 700 hPa and to the Southern Ocean at 300 hPa. It is also noted that at 300 hPa, CMIP5-MMM has overestimated cloud fractions (2.5 — 16%) over the southern Pacific trade-wind regions, indicating that the CMIP5 models tend to simulate too many high clouds over these regions, which might be related to the bias of cloud-radiation-dynamics coupling produced by the lack of precipitating ice radiative effects in the convective regions reported in Li et al. (2021).

In summary, while most of the CMIP5 models do not consider radiatively active precipitating ice and/or convective hydrometeor, we provide estimates of HF for cloud-only (NPCHF) so that a robust estimated HF can be used for model evaluation within the limitations of measurement accuracy, which can vary with cloud and precipitating types that cannot be qualified in this study. The results show that the HF is significantly underestimated in CMIP5 MMM (up to 30 %) against the observational total HF (THF), while the CMIP5 models simulate HF quite well against observational cloud-only HF. The implications of these results on model representations of cloud fraction should include radiatively active precipitating ice and convective hydrometeor types besides the cloud-only type to have a complete model-data comparison for cloud and precipitating ice fraction.

Acknowledgments

The research was carried out at the Jet Propulsion Laboratory, California Institute of Technology, under a contract with the National Aeronautics and Space Administration (80NM0018D0004). This work has been supported primarily by NASA MAP project and in part by the NASA CloudSat, obs4MIPs, and NASA Making Earth System Data Records for Use in Research Environments (MEaSUREs) programs. WLL has been supported by the Ministry of Science and Technology of Taiwan under the contract MOST 110-2111-M-001-008.

The availability of vertically-resolved cloud hydrometeor profiles 2C-ICE (Deng et al., 2010, 2013) is derived from *CloudSat*-CALIPSO (Stephens et al., 2008; Austin et al., 2009; http://www.cloudsat.cira.colostate.edu/).

REFERENCES

Austin, R., and G. L. Stephens (2001), Retrieval of stratus cloud microphysical parameters using millimeter-wave radar and visible optical depth in preparation for Cloudsat: 1. Algorithm formulation, *J. Geophys. Res.*, 106, 28,233– 28,242.

Austin, R. T., A. J. Heymsfield, and G. L. Stephens (2009), Retrieval of ice cloud microphysical parameters using the CloudSat millimeter-wave radar and temperature, *J. Geophys. Res.*, *114*, D00A23, doi:10.1029/2008JD010049.

Bodas-Salcedo, A., M. J. Webb, S. Bony, H. Chepfer, J.-L. Dufresne, S. A. Klein, Y. Zhang, R. Marchand, J. M. Haynes, R. Pincus, and V.O. John, (2011), COSP: Satellite simulation software for model assessment. *Bull. Amer. Meteor. Soc.*, doi: 10.1175/2011BAMS2856.1

Brown, P. R. A., and P. N. Francis (1995), Improved measurements of the ice water content in cirrus using a total-water probe, *J. Atmos. Oceanic Technol.*, 12, 410–414, doi:10.1175/1520-0426(1995)012<0410: IMOTIW>2.0.CO;2.

Cesana, G., Del Genio, A. D., Ackerman, A. S., Kelley, M., Elsaesser, G., Fridlind, A. M., et al. (2019). Evaluating models' response of tropical low clouds to SST forcings using CALIPSO observations. *Atmospheric Chemistry and Physics*, *19*(5), 2813–2832. https://doi. org/10.5194/acp-19-2813-2019.

Cesana, G., Chepfer, H., Winker, D., Getzewich, B., Cai, X., Jourdan, O., Mioche, G., Okamoto, H., Hagihara, Y., Noel, V., and Reverdy, M.: Using in situ airborne measurements to evaluate three cloud phase products derived from CALIPSO: CALIPSO Cloud Phase Validation, J. Geophys. Res.-Atmos., 121, 5788–5808, https://doi.org/10.1002/2015JD024334, 2016.

Chen, W.-T. Chen, C. P. Woods, J.-L. F. Li, D. E. Waliser, J.-D. Chern, W.-K. Tao, J. H. Jiang, and A. M. Tompkins (2011), Partitioning CloudSat Ice Water Content for Comparison with Upper-Tropospheric Ice in Global Atmospheric Models, *J. Geophys. Res.*,doi:10.1029/2010JD015179.

Clothiaux, E. E., Moran, K. P., Martner, B. E., Ackerman, T. P., Mace, G. G., Uttal, T., Mather, J. H., Widener, K. B., Miller, M. A. and Rodriguez, D. J., (1999), The Atmospheric Radiation Measurement program cloud radars: Operational modes. *J. Atmos. Oceanic Tech., 16,* 819–827.

Delanoë, J., and R. J. Hogan (2008), A variational scheme for retrieving ice cloud properties from combined radar, lidar, and infrared radiometer, *J. Geophys. Res.*, 113, D07204, doi:10.1029/2007JD009000.

Delanoë, J., and R. J. Hogan (2010), Combined CloudSat-CALIPSO-MODIS retrievals of the properties of ice clouds, *J. Geophys. Res.*, 115, D00H29, doi:10.1029/2009JD012346.

Del Genio, A. D., M.–S. Yao, W. Kovari, and K. K.–W. Lo (1996), A prognostic cloud water parameterization for global climate models, *J. Climate, 9(2)*, 270–304, doi:10.1175/1520-0442(1996)009<0270:APCWPF>2.0.CO;2.

Deng, M., G. G. Mace, Z. Wang, and H. Okamoto (2010), Tropical Composition, Cloud and Climate Coupling Experiment validation for cirrus cloud profiling retrieval using CloudSat radar and CALIPSO lidar, *J. Geophys. Res.*, 115, D00J15, doi:10.1029/2009JD013104.

Deng, M., G. G. Mace, Z. Wang, and R. P. Lawson (2013), Evaluation of several A-Train ice cloud retrieval products with in situ measurements collected during the SPARTICUS campaign, *J. Appl. Meteor. Climatol., 52,* 1014–1030. doi: 10.1175/JAMC-D-12-054.1.

Francis, P. N., P. Hignett, and A. Macke (1998), The retrieval of cirrus cloud properties from aircraft multi-spectral reflectance measurements during EUCREX'93, *Q. J. R. Meteorol. Soc.*, 124, 1273– 1291.

Gettelman, A., X. Liu, S. J. Ghan, H. Morrison, S. Park, A. J. Conley, S. A. Klein, J. Boyle, D. L. Mitchell, J.-L. F. Li, (2010), Global simulations of ice nucleation and ice supersaturation with an improved cloud scheme in the Community Atmosphere Model. J. *Geophys. Res.,* 115, D18216, doi:10.1029/2009JD013797.

Gettelman, A., and H. Morrison (2015), Advanced two-moment bulk microphysics for global models. Part I: Off-line tests and comparison with other schemes. *J. Climate*, 28(3), 1268–1287, doi:10.1175/JCLI-D-14-00102.1.

Gleckler, P. R. Ferraro, D. E. Waliser (2011), Better use of satellite data in evaluating climate models contributing to CMIP and assessed by IPCC, Meeting Summary, EOS, Vol. 92, No. 20, 17 May 2011.

Hogan, R. J. (2006), Fast approximate calculation of multiply scattered lidar returns, *Appl. Opt.*, 45, 5984–5992.

Hourdin F., I. and coauthors, (2006), The LMDZ4 general circulation model : climate performance and sensitivity to parametrized physics with emphasis on tropical convection. *Climate Dynamics*, 19(15) :3445-3482, DOI : 10.1007/s00382-006-0158-0.

Le Treut, H., and Z. X. Li, (1991), Sensitivity of an atmospheric general circulation model to prescribed SST changes: Feedback effects associated with the simulation of cloud optical properties. *Climate Dyn., 5,* 175–187.

Li, J.-L. F., Gregory V Cesana, Kuan-Man Xu, Mark Richardson, Hanii Takahashi, J. Jiang, (2022), Comparisons of Simulated Radiation, Surface Wind Stress and SST Fields over Tropical Pacific by the GISS CMIP6 Versions of Global Climate Models with Observations, *Environ. Res. Commun.*, IOP, accepted.

Li, J.-L. F., and co-authors, (2022), Observational Evaluation of Global Climate Model Simulations of Arctic Sea Ice Pertaining to the Radiative Effects of Frozen Hydrometeors, *Environ. Res. Commun.* Volume 4, Number 2, 4 025008.

Li, J.-L. F., K.-M. Xu, Wei-Liang Lee, J. H. Jiang, Eric Fetzer, Graeme Stephens, Jia-Yuh Yu, and Yi-Hui Wang, 2021: Changes of south-central Pacific large-scale environment associated with hydrometeors-radiation-circulation interactions in a coupled GCM. *J. Geophys. Res.*, *125*, DOI:10.1029/2021JD034973.

Li, J-L.F., Seungwon Lee, Hsi-Yen Ma, G. Stephens, and Bin Guan, (2018), Assessment of the Cloud Liquid Water from Climate Models and Reanalyses using Satellite Observations, Terrestrial Atmospheric and Oceanic Sciences, DOI: 10.3319/TAO.2018.07.04.01.

Li, J.-L. F., W.-L. Lee, J.-Y. Yu, G. Hulley, E. Fetzer, Y.-C. Chen, and Y.-H. Wang (2016b), The impacts of precipitating hydrometeors radiative effects on land surface temperature in contemporary GCMs using satellite observations, *J. Geophys. Res. Atmos., 120,* doi:10.1002/2015JD023776.

Li, J.-L. F., W.-L. Lee, Tong Lee, Eric Fetzer, Jia-Yuh Yu, (2016a), The Impacts of Cloud Snow Radiative Effects on Pacific Oceans Surface Heat Fluxes, Surface Wind Stress, and Ocean Temperatures in Coupled GCM Simulations, *J. Geophys. Res. Atmos., 120*, DOI: 10.1002/2014JD022538.

Li, J.-L. F., R. M. Forbes, D. E. Waliser, G. Stephens, S. W. Lee, (2014b), Characterizing the impacts of precipitating snow hydrometeors in the radiation using the ECMWF IFS global model, *J. Geophys. Res. Atmos.,* 119, doi:10.1002/2014JD021450.

Li, J.-L. F., W.-L. Lee, D. E. Waliser, J. David Neelin, Justin P. Stachnik, Tong Lee, (2014a), Cloud-Precipitation-Radiation-Dynamics Interaction in Global Climate Models: A Snow and Radiation Interaction Sensitivity Experiment, *J. Geophys. Res. Atmos*., DOI: 10.1002/2013JD021038.

Li, J.-L. F**.,** D. E. Waliser, G. Stephens, S. Lee, T. L'Ecuyer, S. Kato, N. Loeb, and H.-Y. Ma (2013), Characterizing and understanding radiation budget biases in CMIP3/CMIP5 GCMs, contemporary GCM, and reanalysis, *J. Geophys. Res. Atmos., 118,* doi:10.1002/jgrd.50378.

Li, J.-L. F., D. E. Waliser, W.-T. Chen, B. Guan, T. Kubar, G. Stephens, H-Y Ma, D. Ming, L. Donner, C. Seman, and L. Horowitz, (2012), An observationally based evaluation of cloud ice water in CMIP3 and CMIP5 GCMs and contemporary reanalyses using contemporary satellite data, J. Geophys. Res., doi:10.1029/2012JD017640.

Liou, K. K., 1986, Influence of cirrus clouds on weather and climate processes: A global perspective, *Mon. Wea. Rev., 114,* 1167-1198.

Liou, K. N., 2002, An Introduction of Atmospheric Radiation, 2nd Edition, Academic Press, Chapter 8.

Ma, H.-Y.,M. Köhler, J.-L. F. Li, et al., (2012), Evaluation of an ice cloud parameterization based on a dynamical-microphysical lifetime concept using CloudSat observations and the ERAInterim reanalysis, *J. Geophys. Res., 117,* D05210, doi:10.1029/2011JD016275.

Mace, G. G., Q. Zhang, M. Vaughan, R. Marchand, G. Stephens, C. Trepte, and D. Winker (2009), A description of hydrometeor layer occurrence statistics derived from the first year of

merged CloudSat and CALIPSO data, *J. Geophys. Res.*, 114, D00A26, doi:10.1029/2007JD009755.

Michibata, T., K. Suzuki, M. Sekiguchi, and T. Takemura (2019), Prognostic precipitation in the MIROC6-SPRINTARS GCM: Description and evaluation against satellite observations. *J. Adv. Model. Earth Syst., 11,* 839-860. doi:10.1029/2018MS001596.

Ogura, T., S. Emori, M. J. Webb, Y. Tsushima, T. Yokohata, A. Abe-Ouchi, and M. Kimoto, (2008), Towards understanding cloud response in atmospheric GCMs: The use of tendency diagnostics. *J. Meteor. Soc. Japan*, 86, 69–79.

Rasch, P. J., and J. E. Kristjánsson (1998), A comparison of the CCM3 model climate using diagnosed and predicted condensate parameterizations, *J. Climate, 11,* 1587–1614.

Rotstayn, L. D., (1997),A physically based scheme for the treatment of stratiform clouds and precipitation in large-scale models. I: Description and evaluation of the microphysical processes, *Q. J. Roy. Meteorol. Soc.,* 123, 1227-1282, 1997.

Rotstayn, L. D., B. F. Ryan, and J. Katzfey (2000), A scheme for calculation of the liquid fraction in mixed-phase clouds in large-scale models, *Mon. Wea. Rev., 128*, 1070–1088.

Sassen, K., Z. Wang, and D. Liu (2009), Cirrus clouds and deep convection in the tropics: Insights from CALIPSO and CloudSat, *J. Geophys. Res.*, 114, D00H06, doi:10.1029/2009JD011916.

Schumann, U., 2002, Contrail cirrus, In Cirrus, Eds. D. K. Lynch, et al., Oxford University Press, pp.231-255.

534 Song, Xiaoliang, G. J. Zhang1, J-L F. Li (2011), Evaluation of Microphysics Parameterization for
535 Convective Clouds in the NCAR Community Atmosphere Model CAM5, *J. Clim*, Vol. 25,
536 No. 24 (15 December 2012), pp. 8568-8590 (23 pages).

537 Sundqvist, H., E. Berge, and J. E. Kristjánsson, 1989: Condensation and cloud
538 parameterization studies with a mesoscale numerical weather prediction
539 model. *Mon. Wea. Rev.*, **117**, 1641–1657, https://doi.org/10.1175/1520-
540 0493(1989)117<1641:CACPSW>2.0.CO;2.

541 Stein, Thorwald H. M., Julien Delanoë, Robin J. Hogan (2011), A Comparison among Four
542 Different Retrieval Methods for Ice-Cloud Properties Using Data
543 from CloudSat, CALIPSO, and MODIS. *J. Appl. Meteor. Climatol.*, 50, 1952–1969. doi:
544 10.1175/2011JAMC2646.1

545 Stephens, G. L., et al. (2009), CloudSat mission: Performance and early science after the first
546 year of operation, *J. Geophys. Res.*, *113*, D00A18, doi:10.1029/2008JD009982, [printed
547 114(D8), 2009].

548 Sassen, K., and Z. Wang, (2008) Classifying clouds around the globe with the CloudSat radar: 1-
549 year of results, Geophys. Res. Lett., 35, L04805, doi:10.1029/2007GL032591.

550 Taylor, K. E. (2001), Summarizing multiple aspects of model performance in a single diagram, *J.*
551 *Geophys. Res.*, *106*, 7183–7192.

552 Tao, W., J. Chern, Robert Atlas, David Randall, Marat Khairoutdinov, J-L F. Li, Duane E. Waliser,
553 A. Hou, Xin Lin, Christa Peters-Lidard, William Lau, Jonathan Jiang, and J. Simpson,
554 2009: A Multiscale Modeling System: Developments, Applications, and Critical Issues,
555 *Bull. Amer. Meteor. Soc.*, 90(4), 515–534.

556 Tiedtke, M. (1993), Representation of clouds in large-scale models, *Mon. Wea. Rev., 121*, 3040–
557 3061.
558 Volodin, E. M., N. A. Dianskii, and A. V. Gusev, (2010), Simulating Present Day Climate with
559 the INMCM4.0 Coupled Model of the Atmospheric and Oceanic General Circulations,
560 ISSN 0001 4338, Izvestiya, Atmospheric and Oceanic Physics, 2010, Vol. 46, No. 4, pp.
561 414–431.

562 Waliser, D. E., et al. (2009), Cloud ice: A climate model challenge with signs and expectations of
563 progress, *J. Geophys. Res.*, *114*, D00A21, doi:10.1029/2008JD010015.
564 Waliser, D. E., J.–L. F. Li, T. S. L'Ecuyer, and W.–T. Chen (2011), The impact of precipitating
565 ice and snow on the radiation balance in global climate models, *Geophys. Res. Lett., 38*,
566 L06802, doi:10.1029/ 2010GL046478.
567 Wu, L-T and J.-L.-F. Li et al, (2015), An observationally-based evaluation of WRF regional
568 climate simulations over the Central and Eastern Pacific, *J. Geophys.*
569 *Res.,* DOI: 10.1002/2015JD023561.

570 Xu, K.-M., and coauthors, (2002), An intercomparison of cloud-resolving models with the ARM
571 summer 1997 IOP data. *Q. J. Roy. Meteor. Soc., 128*, 593-624.

572 Young, Stuart A., Mark A. Vaughan (2009), The Retrieval of Profiles of Particulate Extinction
573 from Cloud-Aerosol Lidar Infrared Pathfinder Satellite Observations (CALIPSO) Data:
574 Algorithm Description. *J. Atmos. Oceanic Technol.*, 26, 1105–1119. doi:
575 10.1175/2008JTECHA1221.1

576 Zhang, Chengzhu, Minghuai Wang, Hugh Morrison, Richard C. J. Somerville, Kai Zhang,
577 Xiaohong Liu, J.-L. F. Li, (2014), Investigating Ice Nucleation in Cirrus Clouds with an

578 Aerosol-enabled Multi-scale Modeling Framework. *J. Adv. Model. Earth Syst.*, DOI:
579 10.1002/2014MS000343.

580

581

582 **FIGURES**

583

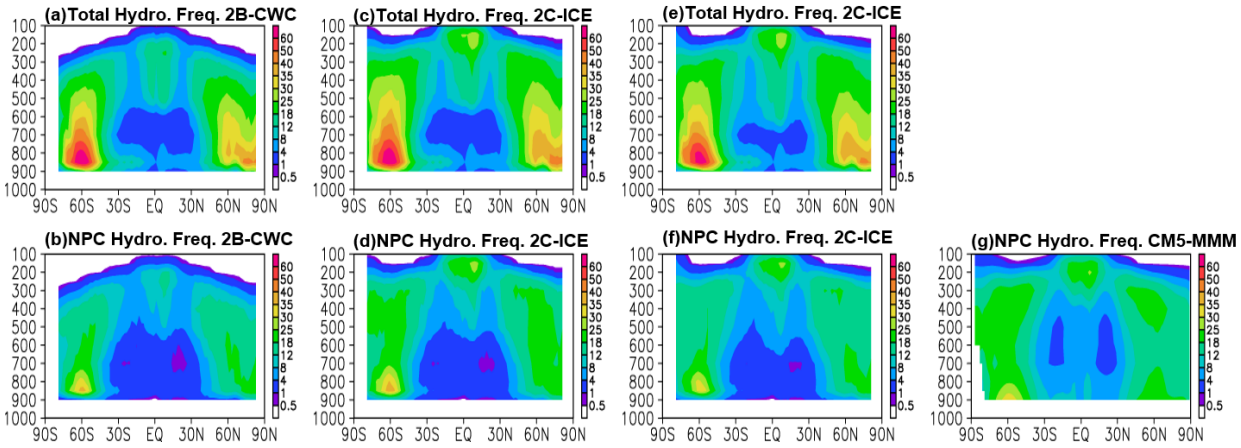

584

585 ***Figure 1. (a)*** Zonally-averaged annual means of total radiatively-active hydrometeor frequency
586 from 2B-CWC data product, (b) same as (a) but for non-precipitating and non-convective
587 hydrometer frequency, which combines floating ice with floating liquid HFs. (c)—(d) same as
588 (a)—(b) but for 2C-ICE data product. (e)—(f) same as (a)—(b) but for DARDAR data product.
589 Floating liquid HF from 2B-CWC is used in (a-f). (g) same as (b) but for CMIP5 multi-model-
590 mean (MMM) cloud fraction in 1980-2005. Units: %.

591

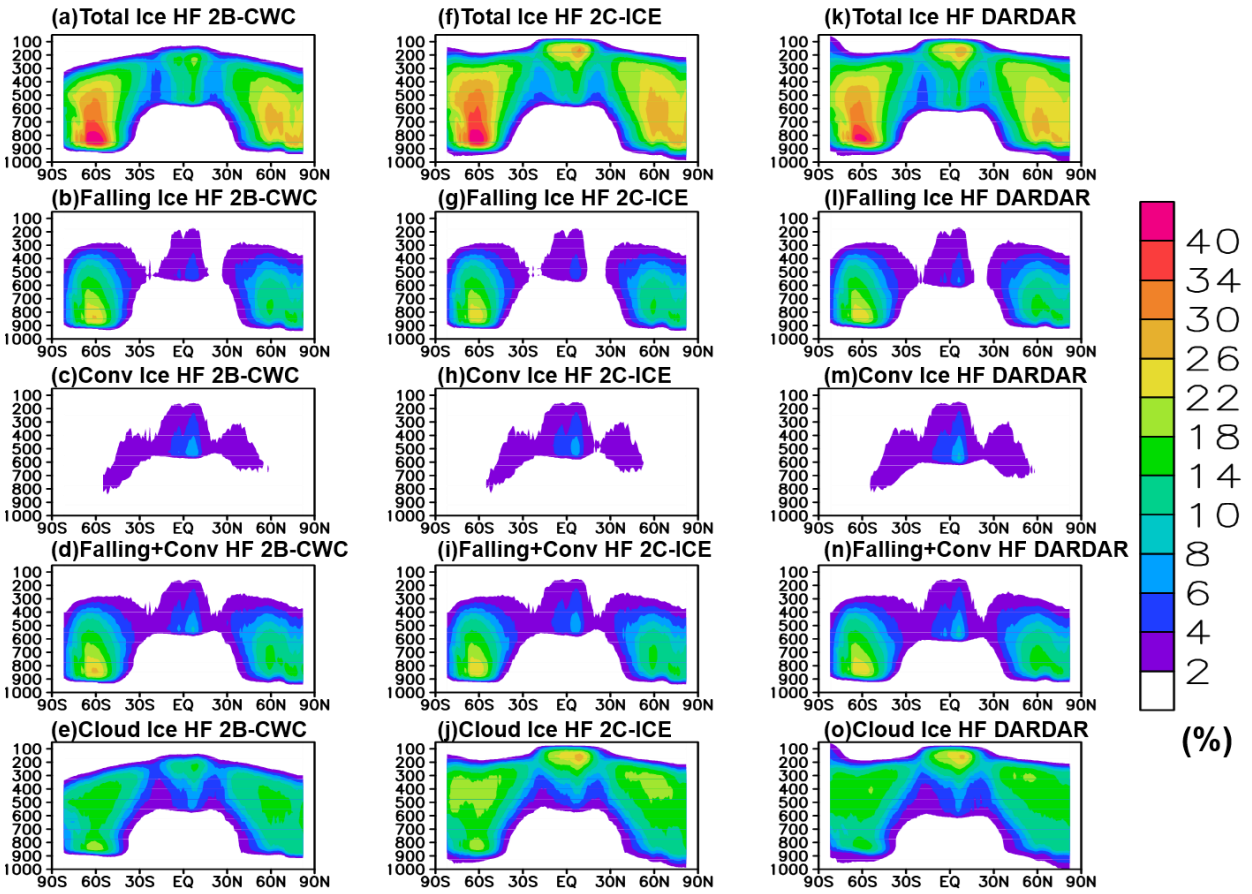

592

593 **Figure 2.** Zonally-averaged annual mean of (a) total ice hydrometeor frequency (TIHF), (b)
594 precipitating ice hydrometeor frequency (PIHF), (c) convective ice hydrometeor frequency
595 (CIHF), (d) sum of precipitating and convective ice hydrometeor frequency and (e) floating ice
596 hydrometeor frequency (FIHF) from 2B-CWC CloudSat radar only; (f)—(j) same as (a)—(e) but
597 for 2C-ICE derived from both the CloudSat radar and CALIPSO lidar; (k)—(n) same as (a)—(e)
598 but from DARDAR derived from both the CloudSat radar and CALIPSO lidar for period of 2007—
599 2010. The hydrometeors frequencies are estimated based on surface precipitation and/or
600 convective cloud flags. See Li et al. (2012) for the details and references for these methods. Unit
601 is %.

602

603 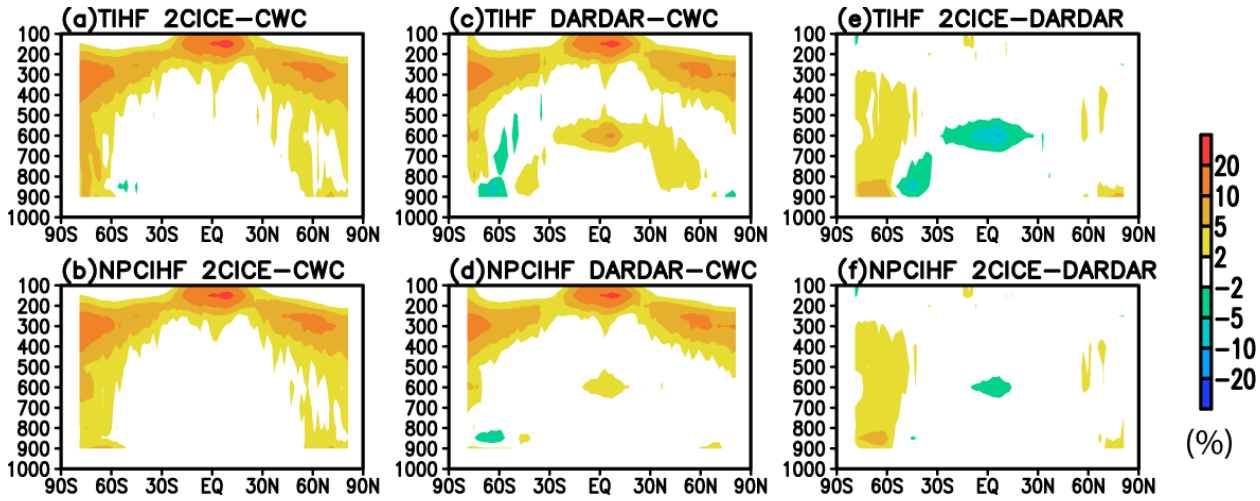

604 ***Figure 3.*** Zonally-averaged annual mean difference of (a) total ice hydrometeor frequency (TIHF)
605 between 2C-ICE and 2B-CWC (CWC), (b) same as (a) but for non-precipitating and non-
606 convective ice hydrometeor frequency (NPCIHF), (c)—(d) same as (a)—(b) but for the difference
607 between DARDAR and 2B-CWC (CWC), (e)—(f) same as (a)—(b) but for the difference between
608 2C-ICE and DARDAR for period of 2007—2010.

609

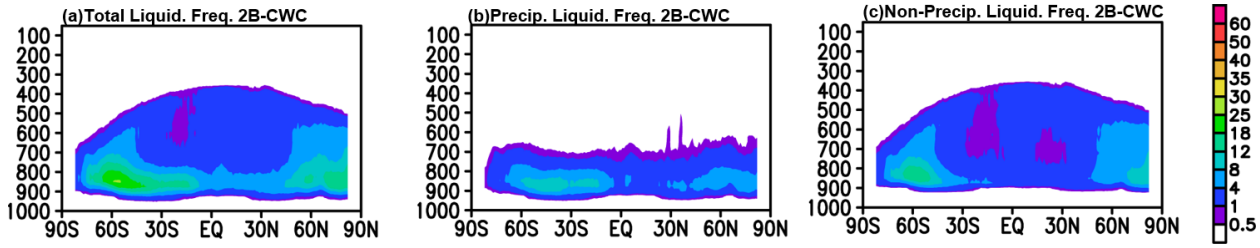

Figure 4. Zonally-averaged annual mean of (a) total liquid hydrometeor frequency (TLHF) which is summed of (b) precipitating liquid hydrometeors (PLHF) and (c) non-precipitating (NPCLHF). Units: %.

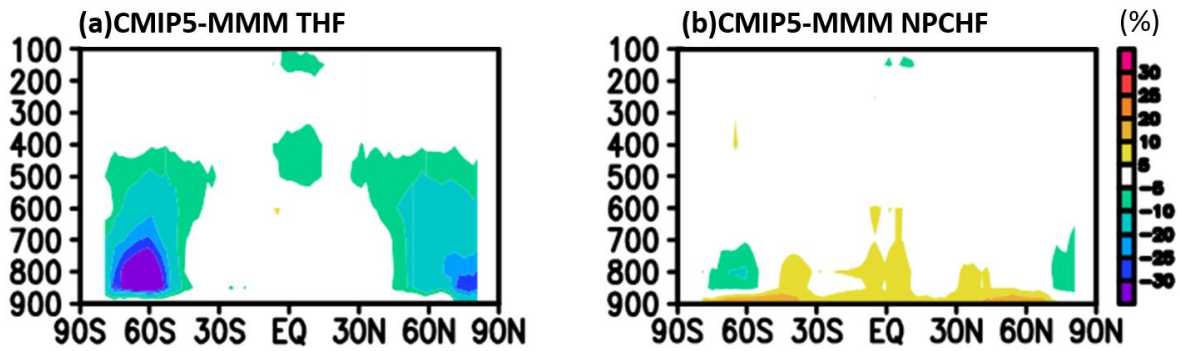

Figure 5. (a) CMIP5 multi-model-mean (CMIP5-MMM) zonally-averaged cloud fraction bias against total hydrometeor frequency (ice+liquid+snow) (TOT) from 2B-CWC +2C-ICE, (b) same as in (a) but against stratiform "cloud only (ice+liquid)" (NPCHF) from 2B-CWC+2C-ICE. Units: %.

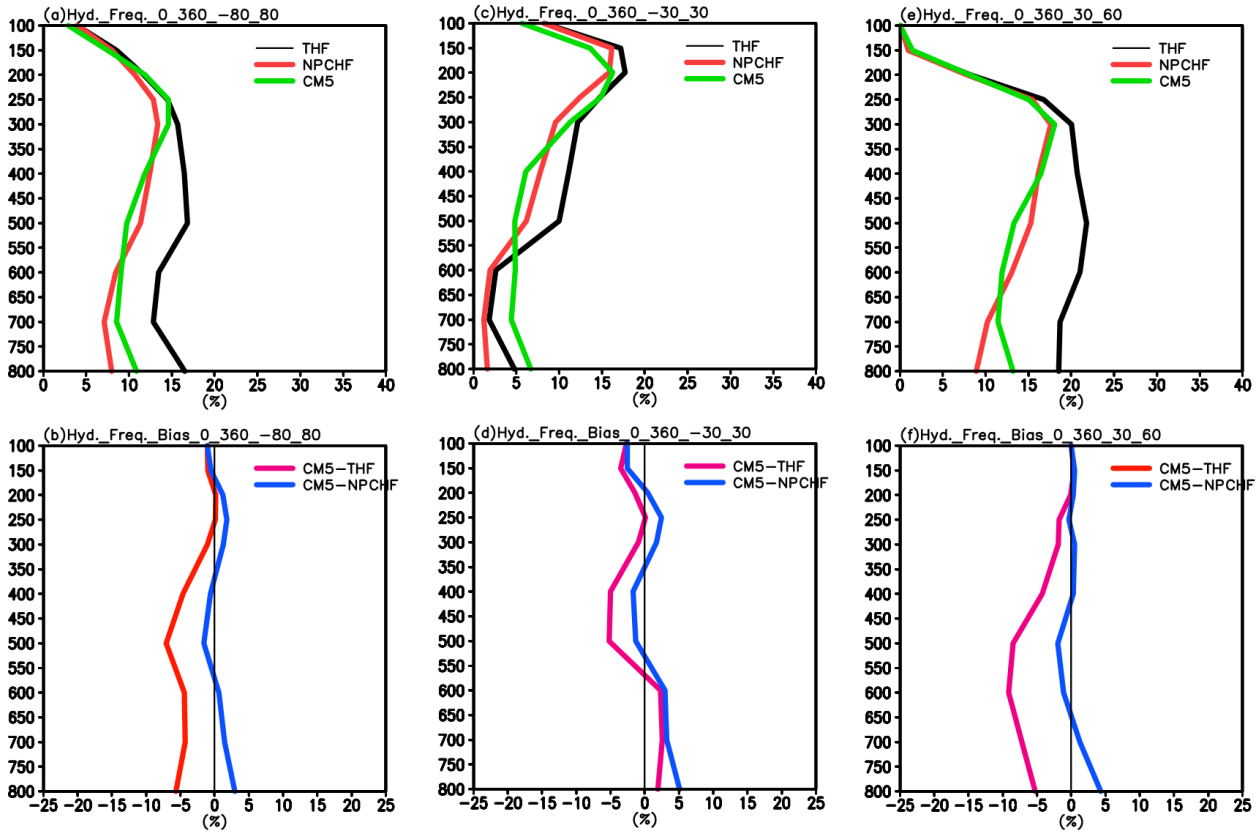

628

629 **Figure 6**. (a) Regional average hydrometeor frequency profiles of total (TOT: red color), non-
630 precipitation and non-convective HF (NPC: blue) and CMIP5-MMM (MMM: black) cloud
631 fraction average over the nearly global domain (80 S – 80N), (b) Same as (a) but for the differences
632 of profile of CMIP5 MMM against NPCHF (blue) and THF (red) estimates; (c)—(d) Same as
633 (a)—(b) but for the area average over the tropics (30 S – 30N); (e)—(f) Same as (a)—(b) but for
634 NH midlatitudes (30 N – 60 N), (g)—(h) Same as (a)—(b) but for SH midlatitudes (30 S – 60 S),
635 (i)—(j) Same as (a)—(b) but for NH high latitudes (60 N – 80 N), (k)—(l) Same as (a)—(b) but
636 for SH high latitudes (60 S – 80 S). Units: %.

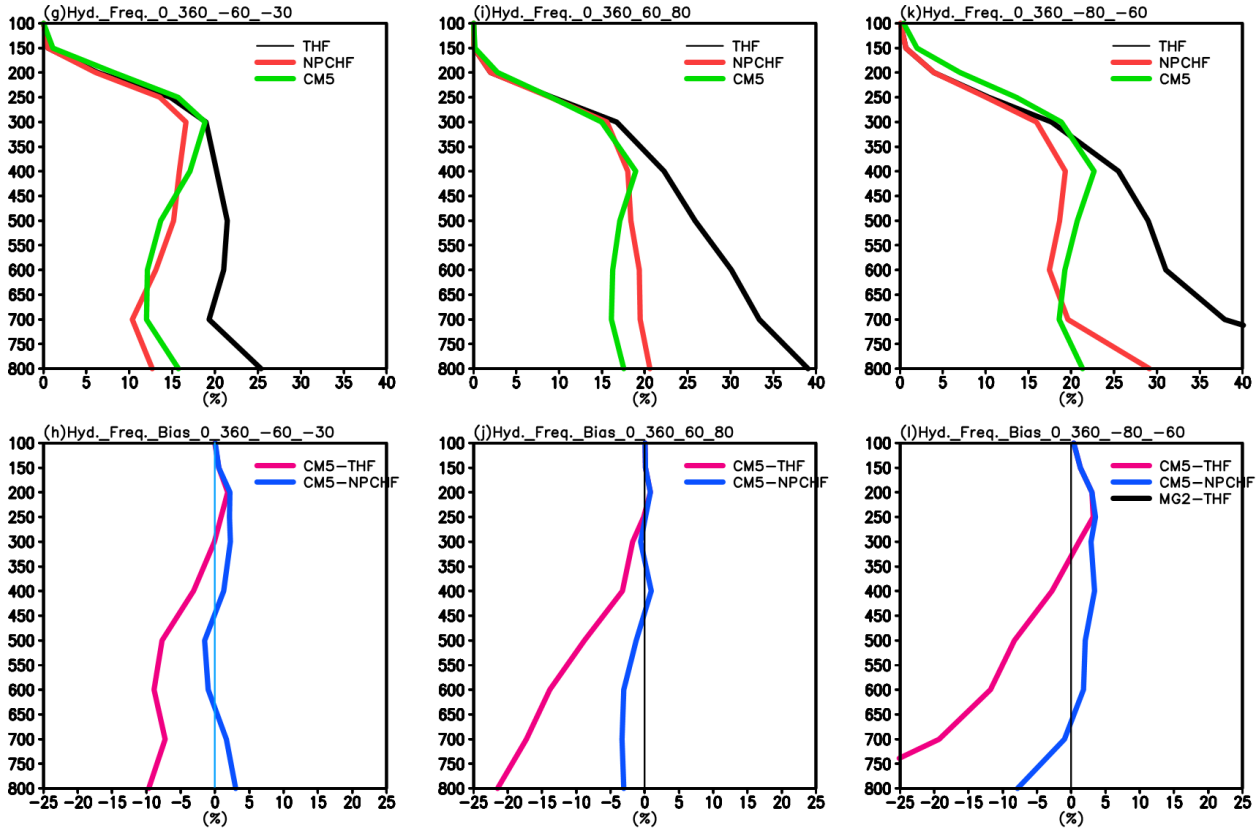

637

638 **Figure 6** continue.

639

640

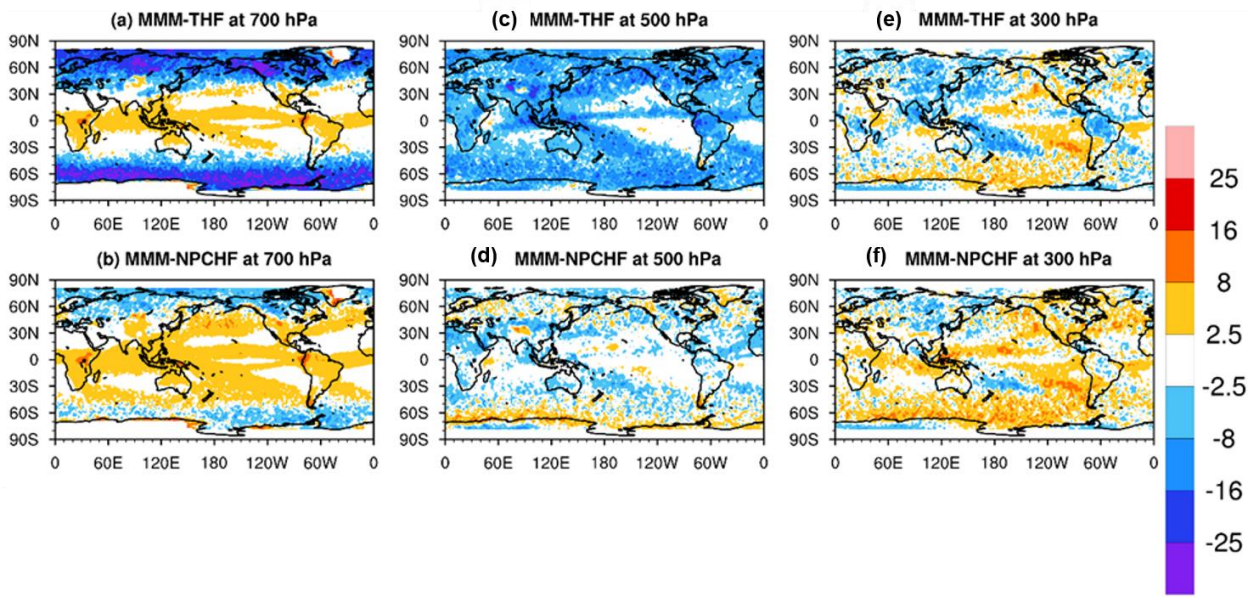

641

642 **Figure 7.** (a) CMIP5 multi-model means (MMM) cloud fraction biases at 700 hPa against the
643 estimated total hydrometeor fraction (THF), (b) same as (a) but against the estimated cloud-only
644 hydrometeor fraction (NPCHF); (c)—(d) same as (a)—(b) but at 500 hPa; (e)—(f) same as (a)—
645 (b) but at 300 hPa. Units: %.

646

APPENDIX

TABLE

Table A1a. Model label, number of model grids, institution and model full name of CMIP5 models examined in this study.

Model Label	**Number of model grids (x, y, and z)**	**Institution/Full Model Name**
GISS-E2-R	90x144x29	NASA / Goddard Institute for Space Studies, USA/GISS-E2-R
Inmcm4	120x180x21	Institute for Numerical Mathematics, Russia/Inmcm4
IPSL	96x96x39	Institute Pierre Simon Laplace, France/IPSL-CM5A-LR
MIROC	64x128x80	University of Tokyo, NIES, and JAMSTEC, Japan/MIROC-ESM-CHEM
MIROC-ESM	64x128x80	University of Tokyo, NIES, and JAMSTEC, Japan/MIROC-ESM
MRI-CGCM3	160x320x35	Meteorological Research Institute, Japan/MRI-CGCM3
NorESM	96x144x26	Norwegian Climate Centre, Norway/NorESM1-M
CSIRO	96x192x18	Australian Commonwealth Scientific and Industrial Research Organization, Australia/CSIRO-Mk3-6-0
MPI-ESM-LR	192x96x47	Max Planck Institute for Meteorology, Germany/MPI-ESM-LR

652 **Table A1b.** Outline of cloud microphysics and cloud fraction parameterizations used in the CMIP5

653 models listed in Table A1a.

Models	Prognostic cloud variables	Bulk single moment or double moment	Cloud fraction (PDF based or Non-PDF based)	References
GISS-E2-R	Single mixing ratio of total water Diagnostic precipitating snow	Bulk single moment; mixing ratio of cloud condensate with temperature dependent partitioning (The bounds are adjustable constants with current settings of ice T = −35ºC and liquid at T = −4ºC over ocean; T = −35ºC and liquid at T = −10ºC over land).	Diagnostic, non-PDF based	*Del Genio et al. (1996)*
Inmcm4	Mixing ratio of cloud liquid and ice	Bulk single moment Large scale condensation in the case of relative humidity exceeds 1.	Diagnostic, non-PDF based	*Volodin et al., (2010)*
IPSL	Single mixing ratio of total water	Bulk single moment; mixing ratio of cloud condensate with temperature dependent partitioning (The bounds are adjustable constants with current settings ice at T = −15º C and liquid at T = 0º C).	Diagnostic PDF based	*Bony and Emanuel (2001)*
MIROC and MIROC-ESM	Mixing ratio of cloud liquid and ice	Bulk single moment; different phases determined by temperature	Diagnostic PDF scheme with minor change for calculating anvil cloud	*Ogura et al. (2008)* *Le Treut and Li, (1991);* *Hourdin et al. (2006)*
MRI-CGCM3	Mixing ratio of cloud liquid and ice	Double moment scheme.	Diagnostic PDF based	*Tiedtke (1993)* *Yukimoto et al. (2011)*
NorESM1	Single mixing ratio of total water	Bulk single moment; mixing ratio of cloud condensate with temperature dependent	Diagnostic, non-PDF based	*Rashe and Kristjánsson (1998)*

		partitioning (The bounds are adjustable constants with current settings ice at T = −40oC and liquid at T = −10oC).		*Zhang et al. (2003)* *Boville et al. (2006)*
CSIRO-Mk3.6.0	Mixing ratio of cloud liquid and ice; Diagnostic precipitating snow	Bulk single moment; ice crystal number concentration is diagnosed; mixing ratio of cloud condensate with temperature dependent partitioning (The bounds are adjustable constants with current settings ice at T = −40ºC);	Diagnostic, non-PDF based	*Rotstayn et al. (1997)* *Rotstayn et al. (2000)*
MPI-ESM-LR	Mixing ratio of cloud liquid and ice		cloud fraction is calculated diagnostically as a function of relative humidity	Sundqvist et al. (1989)

654

655

656

657

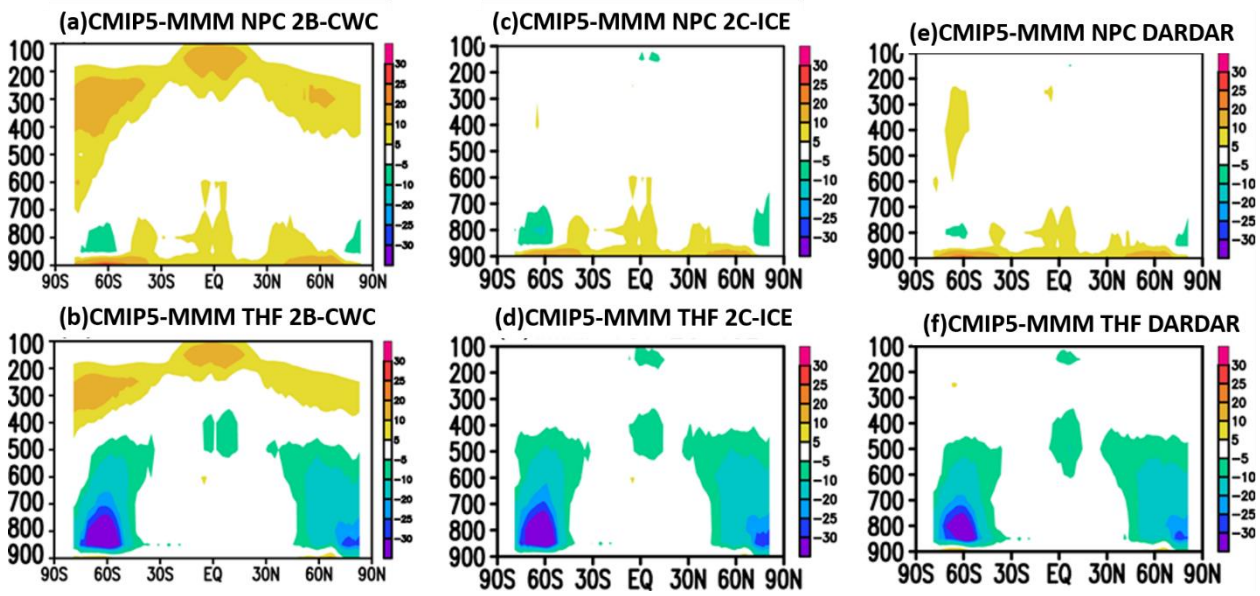

Figure A1. (a) CMIP5 multi-model-mean (MMM) zonally-averaged annual mean cloud fraction biases, compared to non-precipitating and non-convective (NPC) hydrometeor frequency (HF) estimated from 2B-CWC; (b) same as in (a) but against total radiatively-active hydrometeor frequency (ice+liquid+snow) (THF) from 2B-CWC; (c)—(d) same as in (a)—(b) but for 2C-ICE; (e)—(f) same as (a)—(b) but for DARDAR. Units: %.